

Transformations from stripy states to skyrmion crystals

X. R. Wang,^{1,2,*} X. C. Hu,^{1,2} and Z. Z. Sun³

¹*Physics Department, The Hong Kong University of Science and Technology, Clear Water Bay, Kowloon, Hong Kong*

²*HKUST Shenzhen Research Institute, Shenzhen 518057, China*

³*South China Business College, Guangdong University of Foreign Studies, Guangzhou 510545, China*

(Dated: August 2, 2022)

Transformations from condensed stripe skyrmions to skyrmion crystals (SkXs) in perpendicularly magnetized chiral films are investigated in order to clarify a widely spread misconception that stripy phases and SkXs are not topologically connected. Based on our new understanding of skyrmion nature of most stripes in chiral magnetic films, we show that a stripy state, including the helical state, and a SkX are topologically the same. The morphology of a skyrmion condensate is determined only by the ratio of stripe width and skyrmion-skyrmion separation. When stripe width is much smaller than skyrmion-skyrmion separation, the skyrmion condensate is in various stripy phases such as periodically arranged helical states and mazes. The skyrmion condensate has a crystal structure in which individual skyrmions are disk-like objects when stripe width is larger than skyrmion-skyrmion separation. We demonstrated how a collection of given number of stripe skyrmions transforms smoothly and continuously into a SkX no matter whether initial configurations of a set of nucleation domains are randomly or orderly arranged and whether stripe width is gradually or suddenly tuned. This finding does not support the notion of a phase transition from a helical state to a SkX.

I. INTRODUCTION

Magnetic skyrmions have attracted much attention in recent years for their academic interest and potential applications in data storage and processing [1–7]. They are two-dimensional localized topological magnetic textures. Various aspects of magnetic skyrmions have been extensively and intensively studied, including skyrmion characterizations [8–27], generations [28–38], and manipulations [37–45]. Skyrmions and skyrmion crystals (SkXs) can exist in chiral magnets with DMI, or films dominated by dipolar interaction, or films with frustrations.

One recent progress in the field is the recognition of fundamental difference between isolated skyrmions and skyrmion condensates [46, 47]. For a perpendicularly magnetized chiral film described by the magnetization \mathbf{M} , the Heisenberg exchange interaction characterized by stiffness constant A , anisotropic coefficient K , and the Dzyaloshinskii-Moriya interaction (DMI) coefficient D , $\kappa \equiv (\pi^2 D^2)/(16AK)$ is an important quantity and $\kappa = 1$ separates isolated skyrmions ($\kappa < 1$) from condensed stripes ($\kappa > 1$) in the absence of a magnetic field. In contrast to isolated skyrmions that are metastable and disk-like objects when $\kappa < 1$ [12], condensed skyrmions are stripes in nature and are the ground states with negative formation energy when $\kappa > 1$ [46–49], in contrast to the general belief of disk-like objects. Skyrmion condensates can form regular stripy patterns, conventionally called helical or conical states in the literature. However, they often appear as irregular stripy patterns, including maze structures. Recent studies [47, 48] suggest that SkXs can come from a closed packed stripe skyrmions. The width of stripe skyrmions $L \propto A/D$ decreases with D and increases with A , in contrast to the isolated skyrmions

whose size increases with D and decreases with A [12, 48]. Motivated by a widely spread misconception that helical states and SkXs are not topologically connected [50], we study how to use L to continuously transform stripy states to SkXs although smooth transformation between different SkXs were known already [51].

In this paper, we consider perpendicularly magnetized chiral films of $\kappa > 1$. The focus is on morphology or structure transformations of condensed skyrmions at fixed skyrmion density and at fixed $\kappa = 2$ as stripe width varies. We show that condensed skyrmions have all kinds of stripe morphologies when L is smaller than skyrmion-skyrmion separation. As L increases by varying A and K while κ remains unchanged, the condensed skyrmions gradually become SkXs and individual skyrmion becomes a circular spin structure when the stripe width is larger than the skyrmion-skyrmion separation.

II. MODEL AND METHODOLOGY

Our model is an ultra-thin ferromagnetic film in xy plane with the total magnetic energy E consisting of the exchange energy E_{ex} , the DMI energy E_{DM} , the anisotropy energy E_{an} , and magnetic dipolar energy E_{d}

$$E = E_{\text{ex}} + E_{\text{DM}} + E_{\text{an}} + E_{\text{d}}, \quad (1)$$

where $E_{\text{ex}} = Ad \iint |\nabla \mathbf{m}|^2 dS$, $E_{\text{DM}} = Dd \iint [m_z \nabla \cdot \mathbf{m} - (\mathbf{m} \cdot \nabla) m_z] dS$, $E_{\text{an}} = Kd \iint (1 - m_z^2) dS$, and $E_{\text{d}} = \mu_0 M_s d \iint \mathbf{H}_{\text{d}} \cdot \mathbf{m} dS$. M_s , \mathbf{m} , K_u , μ_0 , and d are the magnitude of magnetization or saturation magnetization, the unit direction of \mathbf{M} , the perpendicular magneto-crystalline anisotropy, the vacuum permeability, and film thickness, respectively. Magnetization dynamics is governed by the Landau-Lifshitz-Gilbert (LLG) equation,

$$\frac{\partial \mathbf{m}}{\partial t} = -\gamma \mathbf{m} \times \mathbf{H}_{\text{eff}} + \alpha \mathbf{m} \times \frac{\partial \mathbf{m}}{\partial t}, \quad (2)$$

* Electronic address: phxwan@ust.hk

where γ and α are gyromagnetic ratio and the Gilbert damping constant, respectively. $\mathbf{H}_{\text{eff}} = 2A\nabla^2\mathbf{m} + 2K_u m_z \hat{z} + \mathbf{H}_d + \mathbf{H}_{\text{DM}}$ is the effective field including the exchange field, crystalline anisotropy field, demagnetization field, and DMI field. For very thin film, the demagnetization field can be included in the effective anisotropy $K = K_u - \mu_0 M_s^2/2$, a good approximation when d is much smaller than the exchange length [12]. In this study, our film thickness is maintained at 0.5 nm which is much smaller than the exchange length of $\sqrt{2A/(\mu_0 M_s^2)} > 60$ nm.

TABLE I. The value of material parameters, A , K_u , and K for 10 different films.

| Films | $A(\text{pJ m}^{-1})$ | $K_u(\text{MJ m}^{-3})$ | $K(\text{MJ m}^{-3})$ |
|-------|-----------------------|-------------------------|-----------------------|
| 1 | 1.0 | 0.322 | 0.308 |
| 2 | 1.5 | 0.220 | 0.205 |
| 3 | 2.0 | 0.168 | 0.154 |
| 4 | 2.5 | 0.137 | 0.122 |
| 5 | 3.0 | 0.116 | 0.102 |
| 6 | 3.5 | 0.102 | 0.088 |
| 7 | 4.0 | 0.091 | 0.077 |
| 8 | 4.5 | 0.082 | 0.068 |
| 9 | 5.0 | 0.075 | 0.061 |
| 10 | 5.5 | 0.070 | 0.056 |

In the absence of energy sources such as an electric current and the heat bath, the LLG equation describes a dissipative system whose energy can only decrease [52]. Thus, the steady state solutions of LLG equation with proper initial magnetization distributions are the stable/metastable spin textures of the system Eqs. (1). This is an efficient way to find the morphology of a skyrmion condensate. Mumax3 package [53] is used to search various metastable spin textures in films of $400 \text{ nm} \times 400 \text{ nm} \times 0.5 \text{ nm}$ with periodic boundary conditions in both x and y -directions, and an open boundary condition in the z -direction (or thickness direction). The mesh size is $1 \text{ nm} \times 1 \text{ nm} \times 0.5 \text{ nm}$ so that no change in simulation results is detected when a smaller mesh size is used. In this study, we consider 10 different films with the same $M_s = 0.15 \text{ MA m}^{-1}$ and $D = 1 \text{ mJ m}^{-2}$. A and K_u can vary and are used to tune the stripe width while $\kappa = 2$ are the same for all 10 films. The values of A and K_u , as well as the effective K are listed in Tab. I. A/D of the 10 films varies from 1 nm to 5.5 nm. Also a large $\alpha = 0.5$ is used to speed up our simulations.

III. RESULTS

We first investigate how morphology of 50 skyrmions in chiral magnetic films change with stripe width. According to a previous study [46], each nucleation domain in a chiral magnetic film of $\kappa > 1$ develops into a stripe skyrmion. Thus, 50 nucleation domains of $m_z = 1$ embedded in chiral films of $m_z = -1$ background can

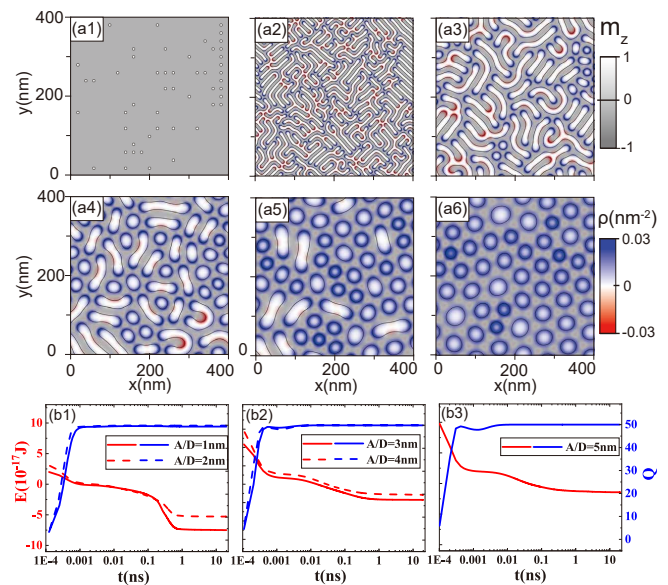


FIG. 1. (a1) Initial configuration of 50 circular nucleation domains of $m_z = 1$ randomly distributed in the films. The diameter of each domain is 6 nm. (a2)-(a6) The stable structures of films with different A/D , starting from initial configuration of (a1). $A/D = 1$ nm (a2), 2 nm (a3), 3 nm (a4), 4 nm (a5), 5 nm (a6), corresponding to Films 1, 3, 5, 7, and 9 in Tab. I. $\kappa = 2$ for all films. (b1)-(b3) The time dependences of skyrmion number Q (the right y-axis and the blue curves) and total magnetic energy E (the left y-axis and the red curves). $A/D = 1$ nm, 2 nm (b1); 3 nm, 4 nm (b2); 5 nm (b3). The time is in the logarithmic scale. All Q reaches the expected integer of 50 within 1 ps, and E approaches its minimum in nanoseconds.

be used to generate 50 skyrmions. The initial diameter of each nucleation domain is 6 nm. In the first two sets of simulations, the 50 domains are initially distributed in films randomly as shown in Fig. 1(a1). Figure 1(a2) is the stable structures of 50 skyrmions in Film 1 with $A/D = 1$ nm (a2). The stripe width is given by $L = a(\kappa)A/D$ with $a(\kappa = 2) = 6.5$ [46], and $L = 6.5$ nm for Film 1 that is more than 8 times smaller than the average skyrmion-skyrmion separation about $\sqrt{400 \times 400/50} \simeq 57$ nm. Since the initial configuration is a random distribution of 50 nucleation domains in the film and each nucleation domain has a large enough space to grow into a ramified stripe skyrmion, and 50 such skyrmions form a dense maze. Figures 1(a3) is a stable structure for Film 3 of $A/D = 2$ nm and the dense maze becomes an irregularly arrange 42 stripe skyrmions and 8 circular-like skyrmions. Figures 1(a4)-1(a6) are stable structures of Film 5 with $A/D = 3$ nm (a4); Film 7 with $A/D = 4$ nm (a5); and Film 9 with $A/D = 5$ nm (a6), all starting from the same initial configuration of Fig. 1(a1).

Indeed, each small domain of initial zero skyrmion number becomes a skyrmion of $Q = \int \rho dx dy = 1$ within 1 picoseconds. $\rho = \frac{1}{4\pi} \mathbf{m} \cdot (\partial_x \mathbf{m} \times \partial_y \mathbf{m})$ is the

skyrmion charge density. Each pattern in Figs. 1(a2)-1(a6) consists of 50 skyrmions, evident from the time-dependence of skyrmion number $Q(t)$ in Figs. 1(b1)-1(b3). $Q(t)$ (the blue or green curves) reaches its final value of 50 within picoseconds. The colours in Fig. 1(a2)-1(a6) encode skyrmion charge distribution. Interestingly, both positive and negative charges appear in a stripe skyrmion while only positive charges exist in a circular skyrmion. Figures 1(a4)-1(a5) are the mixtures of 20 circular skyrmions and 30 stripe skyrmions when $L = 13.02$ nm (a4), 40 circular skyrmions and 10 stripe skyrmions when $L = 26.04$ nm (a5), respectively. SkXs of 50 circular skyrmions form when $2L$ is larger than 57 nm as shown in Fig. 1(a6). The total energy E monotonically decreases with time and approach its minimal values in nanoseconds for all films as shown in Figs. 1(b1)-1(b3) (the left y-axis and the red curves).

Figure 1 demonstrates clearly that the relative values of stripe width and skyrmion-skyrmion separation determines whether the stable structures of collection of skyrmions are stripy pattern or mixture of stripe and circular skyrmions, or SkX with circular skyrmions. In real experiments, one often uses the temperature and other means to tune the materials parameters. To mimic this process, we investigate how a stable stripy structure gradually develop into mixtures of stripe and circular skyrmions and eventually to SkXs consisting of all circular skyrmions as stripe width gradually increases from a value much smaller than skyrmion-skyrmion separation to the values larger than skyrmion-skyrmion separation. In the second set of simulations, starting from the stable spin structure of Fig. 1(a2) with 50 ramified stripe skyrmions in maze structure for Film 1 of $A/D = 1$ nm as the initial configuration, we subsequently increase A by 0.5 pJ m^{-1} and decrease K_u every 20 ns to simulate Films 2 to 10 listed in Tab. I consecutively. 20 ns is long enough for a given system to relax to its new equilibrium state. The criterion for a system in its equilibrium state is that E (as well as Q) does not change with time. Indeed, in our cases, systems reach their equilibrium states within a few nanoseconds as shown in Fig. 2(b). Fig. 2(a1) is the stable structure for $A/D = 1.5$ nm.

Figures 2(a2)-2(a6) are the stable structures for Films 3, 4, 5, 7, and 9, respectively. Each of them is developed from the stable structure of its predecessor. The evolution of both skyrmion number and total magnetic energy are plotted in Fig. 2(b). The results shows no change of skyrmion number as expected from the topological nature of the quantity while the total magnetic energy decreases with time immediately after the new model parameters are used in the simulation. Fig. 2(b) shows also that the system reaches its new stable structures in a few nanoseconds. Compare Fig. 2(a2) with Fig. 1(a3) for Film 3, Fig. 2(a4) with Fig. 1(a4) for Film 5, and Fig. 2(a5) with Fig. 1(a5) for Film 7, each pair shows similar, but not identical, stable structures. The results reveal the fact of a large number of metastable structures for a collection of stripe skyrmions. Which metastable struc-

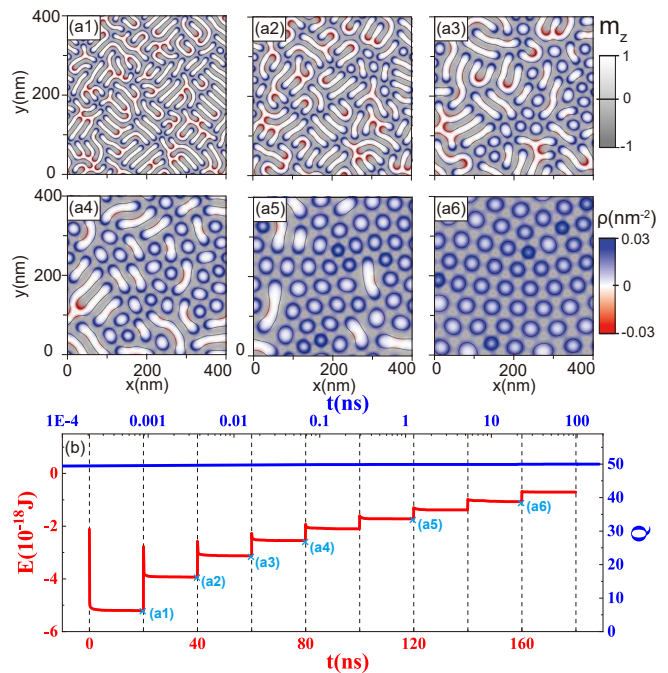


FIG. 2. (a1) Stable structure of Film 2 developed from the stable structure of Film 1 of Fig. 1(a2). The stable structures of the consecutive tuning of model parameters for Film 3 of $A/D = 2$ nm (a2); Film 4 of 2.5 nm (a3); Film 5 of 3 nm (a4); Film 7 of 3.5 nm (a5); Film 9 of 4 nm (a6). $\kappa = 2$ is for all films. (b) The skyrmion number Q (the right y-axis, up x-axis and the blue curves where time is in the logarithmic scale) and total energy E (the left y-axis, down x-axis and the red curves where time is in the normal scale) evolved with time. E for structures of (a1)-(a6) are marked by cross. Q reaches 50 within 1 ps and keep 50 unchanged. E approaches a constant in nanoseconds after changing the parameter.

ture that a mixture of circular and stripe skyrmions ends up depends on the history of the system.

Different from large number of metastable structures of condensed skyrmions containing stripes, the variation of SkXs is limited to collective shift of skyrmion centres within a cell. This explains why SkXs in Figs. 2(a6) and 1(a6) are almost the same although their kinetic and dynamical process are not the same. To further verify the independence of SkXs on their initial configurations, we repeat the similar simulations as that in Fig. 2, but the first stable structure for Film 1 is from the evolution of an initial configuration shown in Fig. 3(a1) where 50 nucleation domains of $m_z = 1$ in the background of $m_z = -1$ are arranged in 2 well ordered columns. Each domain is exactly the same as those for Fig. 1. Figure 3(a2) is the stable helical state after 20ns evolution. Same as before, each nucleation domain develop into a stripe skyrmion that explains $Q(t)$ approaching 50 within picoseconds in Figure 3(b). Stripes tilt about 56° from the y -direction. The stripe tilt comes from film tilting by 25 stripes of width $L \simeq 6.5$ nm. The tilted angle θ satisfies $2L/(\sin \theta) = 400/25$. For $L = 6.5$ nm,

$\theta = \cos^{-1}(13/16) \simeq 54^\circ$, very close to the observed value of 56° . To increase L while keep $\kappa = 2$ unchanged, we increase A by 0.5 pJ m^{-1} and decrease K_u accordingly with the values given in Tab. I every 20 ns. Figures 3(a3)-3(a6) are stable structures for Film 3 with $A/D = 2 \text{ nm}$ at 60 ns (a3), Film 5 with $A/D = 3 \text{ nm}$ at 100 ns (a4), Film 7 with $A/D = 4 \text{ nm}$ (a5), and Film 9 with $A/D = 5 \text{ nm}$ (a6). Figure 3(b) shows how total energy E (the left y-axis, the bottom x-axis and the red curves where time is in the logarithmic scale) and Q (the right y-axis, the top x-axis and the blue curves where time is in the linear scale) vary with time. Q maintains the value of 50 after the first a few picoseconds while E reaches its minimal value in nanoseconds every time after parameters are changed. The number of stripe skyrmions decreases as L increases. All skyrmions in Fig. 3(a6) have circular shape when L is larger than the average skyrmion-skyrmion separation.

In our previous studies [46–49], we showed that spin distribution across stripe skyrmions can be described well by $m_z(x) = \frac{\sinh^2(L/2w) - \sinh^2(x/w)}{\sinh^2(L/2w) + \sinh^2(x/w)}$ for $-L/2 < x < L/2$ and $m_z(x) = -\frac{\sinh^2(L/2w) - \sinh^2(x/w - L/w)}{\sinh^2(L/2w) + \sinh^2(x/w - L/w)}$ for $L/2 < x < 3L/2$, where L and w are the stripe width and wall thickness of stripe skyrmions. $x = 0$ refers to stripe center where $m_z = \pm 1$. Here we test how good the spin profile is for our stripe skyrmions. Figures. 3(c1)-3(c4) are the distributions of m_z crossing those stripes labelled by the green ① in Figs. 3(a2)-3(a5). The y -axis is m_z and $x = 0$ is the stripe centre where $m_z = 1$. Symbols are numerical data across stripes ① and ② (c1); ③ and ④ (c2); ⑤ and ⑥ (c3); and ⑦ and ⑧ (c4). The solid curves are the theoretical spin profile of $m_z = \frac{\sinh^2(L/2w) - \sinh^2(x/w)}{\sinh^2(L/2w) + \sinh^2(x/w)}$ for $-L/2 < x < L/2$ and $m_z = -\frac{\sinh^2(L/2w) - \sinh^2(x/w - L/w)}{\sinh^2(L/2w) + \sinh^2(x/w - L/w)}$ for $L/2 < x < 3L/2$ with $L = 6.51 \text{ nm}$ and $w = 1.73 \text{ nm}$ for (c1); $L = 13.02 \text{ nm}$ and $w = 3.46 \text{ nm}$ for (c2); $L = 19.53 \text{ nm}$ and $w = 5.19 \text{ nm}$ for (c3); $L = 26.04 \text{ nm}$ and $w = 6.92 \text{ nm}$ for (c4). L agrees perfectly with $L = 6.51A/D$ for $\kappa = 2$. Data from different stripes falling onto the same curve demonstrates that stripes, building blocks of pattern, are identical. Although initial configurations in Figs. 1, 2, and 3 are different, and the morphologies of the mixtures of stripe and circular skyrmions are sensitive to initial configuration and their dynamical paths, the structures of SkXs do not depend on the dynamical paths and depend only on the ratio of the stripe width and skyrmion-skyrmion separation.

To further substantiate the assertion above, we carry out similar simulations as those for Fig. 2, but with 100 randomly distributed nucleation domains as the initial configuration. As mentioned before, we should have 100 skyrmions in the system and the average skyrmion-skyrmion separation is reduced to $\sqrt{400 \times 400/100} = 40 \text{ nm}$. Thus, we should expect transformation from maze at $A/D = 1 \text{ nm}$ to the mixture of stripe and circular skyrmions at a smaller $1.5 \text{ nm} \leq A/D < 3.1 \text{ nm}$ than

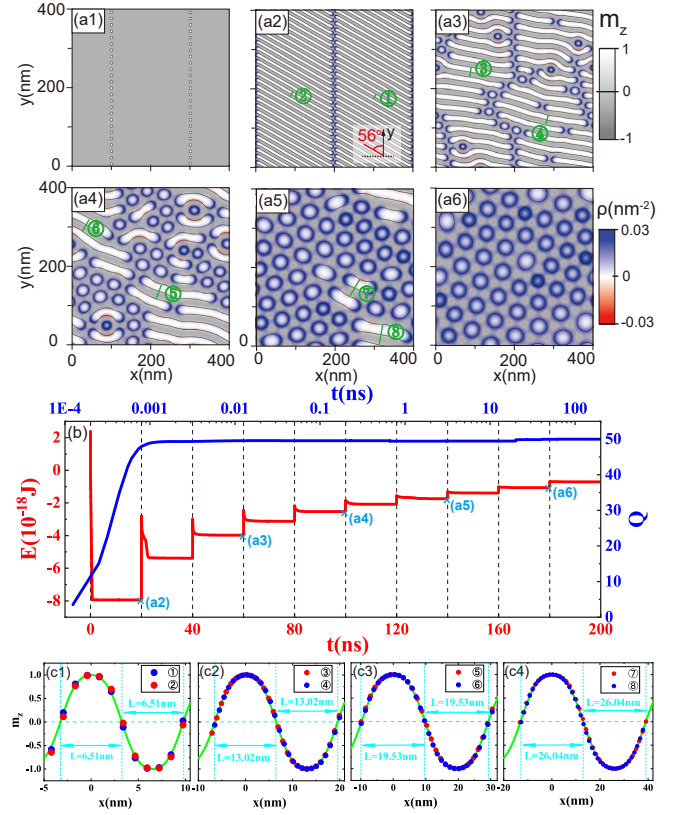


FIG. 3. (a1) Initial configuration of 50 circular nucleation domains of $m_z = 1$ arranged orderly in two columns. The diameter of each domain is 6 nm . (a2-a6) The stable structures for $A/D = 1 \text{ nm}$ (a2); 2 nm (a3); 3 nm (a4); 4 nm (a5); and 5 nm (a6). $\kappa = 2$ is for all films. (b) The time evolution of skyrmion number Q (the right y-axis, the top x-axis and the blue curves where time is in the logarithmic scale) and total energy E (the left y-axis, the bottom x-axis and the red curves where time is in the linear scale). Q reaches 50 within 1 ps and keep this value afterwards even when the parameters are tuned to different values. E for structures of (a2)-(a6) are marked by cross. (c1)-(c4) The red and the blue points are the z -component of magnetization along the green lines labelled by circled n in (a2)-(a5). The green lines are the fit to our approximate profile. The cyan arrows indicate the stripe widths of $m_z < 0$ or $m_z > 0$.

those in Fig. 2 and eventually to a SkX when A/D is larger than $40/(2 \times 6.5) \simeq 3.1 \text{ nm}$. As shown in Fig. 4, (a1) is the initial configuration of 100 circular nucleation domains of $m_z = 1$ in the background of $m_z = -1$ randomly distributed in the film. Same as before, each domain is 6 nm in diameter. (a2) is the stable structure of Film 1 of $A/D = 1 \text{ nm}$ and $\kappa = 2$ after 20 ns evolution. Clearly, it is a maze, and individual skyrmion is an irregular ramified stripe, or a curved stripe, or a short stripe. Their skyrmion nature is revealed from constant value of $Q = 100$ within a picoseconds. At $t = 20 \text{ ns}$, A and K_u are changed to the values of Film 2, and structure in 4(a2) quickly relaxes to a new stable structure shown in 4(a3) at $t = 40 \text{ ns}$ with various types

of stripe skyrmions as well as a few circular skyrmions. We then increase A by 0.5 pJ m^{-1} every 20 ns according to the parameters of Films 3 to 10 given in Tab. I. Figures 4(a4)-4(a9) are stable structures of 100 skyrmions at $t = 60 \text{ ns}$; 80 ns ; 100 ns ; 120 ns ; 140 ns ; and 160 ns respectively for $A/D = 2 \text{ nm}$ (a4); 2.5 nm (a5); 3 nm (a6), 3.5 nm (a7), 4 nm (a8), and 4.5 nm (a9) with stripe width $L = 6.51 \text{ nm}$, 9.76 nm , 13.02 nm , 16.27 nm , 19.53 nm , 22.78 nm , 26.04 nm , 29.29 nm . Indeed, 100 skyrmions form SkXs when $A/D > 3 \text{ nm}$ as shown in Figs. 4(a7)-4(a9). For $A/D = 3 \text{ nm}$, almost all skyrmions are circular except 9 very short stripe skyrmions (a6). Figure 4(b) is the time dependences of total energy E (the left y-axis, the lower x-axis and the red curves. t is in the logarithmic scale) and Q (the right y-axis, the upper x-axis and the blue curves. t is in the linear scale). Q maintains the number of 100 even when model parameters are changed and spin structures are not the steady state solutions any more. It demonstrates clearly the topological feature of the quantity and its resilience to environmental change. E approach its minimal value in nanoseconds every time after parameter tuning.

IV. DISCUSSIONS AND CONCLUSIONS

In this study, only SkXs originated from a collection of stripe skyrmions are considered. This type of SkXs is the subject of the most studies, if not all, in the literature. Essentially, one starts from a skyrmion condensate, a collection of various stripes, and try to increase skyrmion number through the help of thermal agitation and magnetic field [49] or through the external stimulus [48]. Obviously, approach here differs from previous studies in which skyrmion number are kept the same and stripe width is controlled.

The transformations from stripy states to SkXs is smooth and continuous for the type of SkXs studied here. This result does not support the general belief of a sudden first-order or continuous phase transitions between ordered or randomly distributed stripe skyrmions to SkXs. Another type of SkXs is from the closely-packed isolated meta-stable circular skyrmions. Our results may not be applicable to this type of SkXs because of different physics involved. The similarities and differences between the two types of SkXs should be an interesting issue deserved a careful study. SkXs from a collection of isolated skyrmions due to the skyrmion-skyrmion interaction has many similarities with the formation of atomic crystals through atom-atom interactions. It is well known that the melting or crystallization of an atomic crystal to or from a liquid or an amorphous material is the first order phase transition involving latent heat.

It is well known that most magnetic material parameters have strong temperature dependence, especially near the Curie temperature. Thus, the results found here can either be tested by real experiments or used to explain

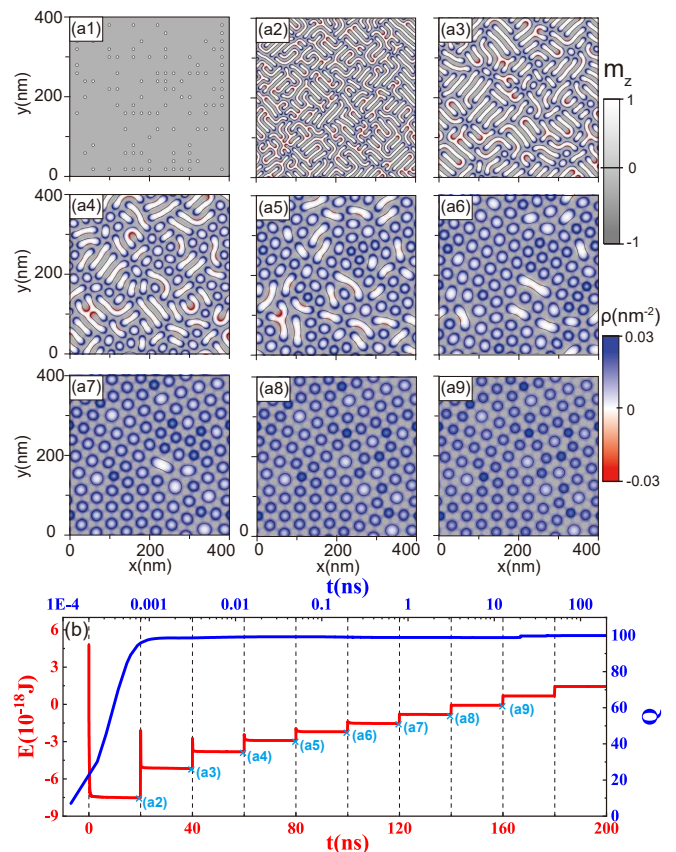


FIG. 4. (a1) The initial configuration with 100 randomly distributed nucleation domains of $m_z = 1$ in the films. The diameter of each domain is 6 nm. (a2)-(a9) The stable structures for $A/D = 1 \text{ nm}$ at $t = 20 \text{ ns}$ (a2); 1.5 nm at $t = 40 \text{ ns}$ (a3); 2 nm at $t = 60 \text{ ns}$ (a4); 2.5 nm at $t = 80 \text{ ns}$ (a5); 3 nm at $t = 100 \text{ ns}$ (a6); 3.5 nm at $t = 120 \text{ ns}$ (a7); 4 nm at $t = 140 \text{ ns}$ (a8); 4.5 nm at $t = 160 \text{ ns}$ (a9). $\kappa = 2$ is for all films. (b) The time-dependence of skyrmion number Q (the right y-axis, the upper x-axis and the blue curves where time t is in the logarithmic scale) and total energy E (the left y-axis, the lower x-axis and the red curves where time t is in the linear scale). E for structures of (a2)-(a9) are marked by cross. Q reaches 100 within 1 ps and remains this value even when model parameters are tuned. E approaches its minimal value in nanoseconds after model parameters are tuned.

experimental observations related to transformations between stripy phases and SkXs. Of course, all parameters vary with the temperature such that both L and κ change with the temperature [54, 55], in contrast to studies here that κ is purposely kept unchanged. It should be pointed out that many recent experiments [54, 55] showed that A and D depends on M very differently although mean field theory conjectured that both A and D vary with M in the same way. Since skyrmion structures are determined by the ratio of L and skyrmion-skyrmion separation, not on κ as long as it supports condensed skyrmion phase ($\kappa > 1$) such that whether κ is a constant or not is not essential as long as $\kappa > 1$. Beside the temperature, other external knobs such electrical fields, magnetic fields, as

well as strains can also change L [56–60]. In fact, using tools other than the temperature may also avoid possible complication from thermal agitation that can change skyrmion number.

In conclusion, a collection of skyrmions transforms into a SkX as the width of stripe skyrmions becomes larger than the skyrmion-skyrmion separation, no matter whether the initial configuration of skyrmions are ordered or randomly distributed in a film and whether the width increases gradually or suddenly. Since the SkX comes from the skyrmion-skyrmion repulsion, it explains why individual skyrmion in a SkX is not a truly circular

spin texture. Our finding does not support the notion of phase transition for SkX formation.

V. ACKNOWLEDGEMENT

This work is supported by the National Key Research and Development Program of China 2020YFA0309600, the National Natural Science Foundation of China (Grant No. 11974296) and Hong Kong RGC Grants (No. 16301518, 16301619, 16302321, and 16300522).

-
- [1] A. N. Bogdanov and U. K. Röbner, *Phys. Rev. Lett.* **87**, 037203 (2001).
- [2] U. K. Röbner, A. N. Bogdanov, and C. Pfeleiderer, *Nature* **442**, 797 (2006).
- [3] S. Mühlbauer, B. Binz, F. Jonietz, C. Pfeleiderer, A. Rosch, A. Neubauer, G. Georgii, and P. Böni, *Science* **323**, 915 (2009).
- [4] X. Z. Yu, Y. Onose, N. Kanazawa, J. H. Park, J. H. Han, Y. Matsui, N. Nagaosa, and Y. Tokura, *Nature* **465**, 901 (2010).
- [5] X. Z. Yu, N. Kanazawa, Y. Onose, K. Kimoto, W. Z. Zhang, S. Ishiwata, Y. Matsui, and Y. Tokura, *Nat. Mater.* **10**, 106 (2011).
- [6] A. Fert, V. Cros, and J. Sampaio, *Nat. Nanotech.* **8**, 152 (2013); J. Sampaio, V. Cros, S. Rohart, A. Thiaville, and A. Fert, *ibid.* **8**, 839 (2013).
- [7] N. Nagaosa and Y. Tokura, *Nat. Nanotech.* **8**, 899 (2013).
- [8] Y. Onose, Y. Okamura, S. Seki, S. Ishiwata, and Y. Tokura, *Phys. Rev. Lett.* **109**, 037603 (2012).
- [9] H. S. Park *et al.*, *Nat. Nanotech.* **9**, 337 (2014).
- [10] S. Krause and R. Wiesendanger, *Nat. Mater.* **15**, 493 (2016).
- [11] S. Rohart and A. Thiaville, *Phys. Rev. B* **88**, 184422 (2013).
- [12] X. S. Wang, H. Y. Yuan, and X. R. Wang, *Commun. Phys.* **1**, 31 (2018).
- [13] X. Gong, H. Y. Yuan, and X. R. Wang, *Phys. Rev. B* **101**, 064421 (2020).
- [14] X. Gong, K. Y. Jing, J. Lu, and X. R. Wang, *Phys. Rev. B* **105**, 094437(2022).
- [15] A. O. Lenov, T. L. Monchesky, N. Romming, A. Kubetzka, A. N. Bogdanov, and R. Wiesendanger, *New J. Phys.* **18**, 065003 (2016).
- [16] H.-B. Braun, *Phys. Rev. B* **50**, 16485 (1994).
- [17] A. Siemens, Y. Zhang, J. Hagemester, E. Y. Vedmedenko, and R. Wiesendanger, *New. J. Phys.* **18**, 045021 (2016).
- [18] E. Simon, K. Palotás, L. Rózsa, L. Udvardi, and L. Szunyogh, *Phys. Rev. B* **90**, 094410 (2014).
- [19] E. A. Karhu, U. K. Röbner, A. N. Bogdanov, S. Kahwaji, B. J. Kirby, H. Fritzsche, M. D. Robertson, C. F. Majkrzak, and T. L. Monchesky, *Phys. Rev. B* **85**, 094429 (2012).
- [20] J. Iwasaki, M. Mochizuki, and N. Nagaosa, *Nat. Commun.* **4**, 1463 (2013).
- [21] S.-Z. Lin, C. Reichhardt, C. D. Batista, and A. Saxena, *Phys. Rev. B* **87**, 214419 (2013).
- [22] W. Koshibae and N. Nagaosa, *Sci. Rep.* **8**, 6238 (2018).
- [23] R. Juge *et al.*, *J. Magn. Magn. Mater.* **455**, 3 (2018).
- [24] J.-V. Kim and M. -W. Yoo, *Appl. Phys. Lett.* **110**, 132404 (2017).
- [25] S. Hoshino and N. Nagaosa, *Phys. Rev. B* **97**, 024413 (2018).
- [26] S. Woo *et al.*, *Nat. Commun.* **9**, 959 (2018).
- [27] S. Woo *et al.*, *Nat. Mater.* **15**, 501 (2016).
- [28] H. Y. Yuan and X. R. Wang, *Sci. Rep.* **6**, 22638 (2016).
- [29] Y. Zhou and M. A. Ezawa, *Nat. Commun.* **5**, 4652 (2014).
- [30] W. Jiang *et al.*, *Science* **349**, 283 (2015).
- [31] J. Li *et al.*, *Nat. Commun.* **5**, 4704 (2014).
- [32] S. Heinze, K. von Bergmann, M. Menzel, J. Brede, A. Kubetzka, R. Wiesendanger, G. Bihlmayer, and Stefan Blügel, *Nat. Phys.* **7**, 713 (2011).
- [33] P. Dürrenfeld, Y. Xu, J. Åkerman, and Y. Zhou, *Phys. Rev. B* **96**, 054430 (2017).
- [34] N. Vidal-Silva, A. Riveros, and J. Escrig, *J. Magn. Magn. Mater.* **443**, 116 (2017).
- [35] M. N. Wilson, A. B. Butenko, A. N. Bogdanov, and T. L. Monchesky, *Phys. Rev. B* **89**, 094411 (2014).
- [36] N. Romming, A. Kubetzka, C. Hanneken, K. von Bergmann, and R. Wiesendanger, *Phys. Rev. Lett.* **114**, 177203 (2015).
- [37] H. Du *et al.*, *Nat. Commun.* **6**, 8504 (2015).
- [38] N. Romming, C. Hanneken, M. Menzel, J. E. Bickel, B. Wolter, K. von Bergmann, A. Kubetzka, and R. Wiesendanger, *Science* **341**, 636 (2013).
- [39] C. Reichhardt, D. Ray, and C. J. Olson Reichhardt, *Phys. Rev. Lett.* **114**, 217202 (2015).
- [40] H. Y. Yuan, X. S. Wang, Man-Hong Yung, and X. R. Wang, *Phys. Rev. B* **99**, 014428 (2019).
- [41] W. Jiang *et al.*, *Nat. Phys.* **13**, 162 (2017).
- [42] S. Jaiswal *et al.*, *Appl. Phys. Lett.* **111**, 022409 (2017).
- [43] K. Litzius *et al.*, *Nat. Phys.* **13**, 170 (2017).
- [44] C. Reichhardt and C. J. Olson Reichhardt, *New J. Phys.* **18**, 095005 (2016).
- [45] J. Sampaio, V. Cros, S. Rohart, A. Thiaville, and A. Fert, *Nat. Nanotech.* **8**, 839 (2013).
- [46] X. R. Wang, X. C. Hu, and H. T. Wu, *Commun. Phys.* **4**, 142 (2021).
- [47] H. T. Wu, X. C. Hu, K. Y. Jing, and X. R. Wang, *Commun. Phys.* **4**, 210 (2021).

- [48] H. T. Wu, X. C. Hu, and X. R. Wang, *Science China* **65**, 247512 (2022).
- [49] X. C. Hu, H. T. Wu, and X. R. Wang, *Nanoscale* **14**, 7516 (2022).
- [50] Back, C. *et al.* The 2020 skyrmionics roadmap. *J. Phys. D: Appl. Phys.* **53**, 363001 (2020).
- [51] K. Karube *et al.*, *Nat. Mat.* **15**, 1237 (2016).
- [52] X. R. Wang, P. Yan, J. Lu, and C. He, *Ann. Phys. (NY)* **324**, 1815 (2009).
- [53] A. Vansteenkiste, J. Leliaert, M. Dvornik, M. Helsen, F. Garcia-Sanchez, and F. B. V. Waeyenberge, *AIP Adv.* **4**, 107133 (2014).
- [54] Y. Zhang, X. Kong, G. Xu, Y. Jin, C. J. Jiang, and G. Z. Chai, *J. Phys. D: Appl. Phys.* **55**, 195304 (2022).
- [55] W. S. Ham, M. Ishibashi, K. Kim, S. Kim, and T. Ono, *J. Phys. D: Appl. Phys.* **61**, 020901 (2022).
- [56] M. Schott, Ranno L., H. Béa, C. Baraduc, S. Auffret, and A. Bernard-Mantel, *J. Magn. Magn. Mater.* **520**, 167122 (2021).
- [57] T. Srivastava *et al.*, *Nano Lett.* **18**, 4871 (2018).
- [58] C. Deger, *Sci. Rep.* **10**, 1 (2020).
- [59] Z. V. Gareeva, A. K. Zvezdin, L. A. Kalyakin, and T. T. Gareev, *J. Magn. Magn. Mater.* **515**, 167255 (2020).
- [60] O. G. Udalov and I. S. Beloborodov, *Phys. Rev. B* **102**, 134422 (2020).